REPORT DOCUMENTATION PAGE		*Form Approved* *OMB No. 0704-0188*

Public reporting burden for this collection of information is estimated to average 1 hour per response, including the time for reviewing instructions, searching existing data sources, gathering and maintaining the data needed, and completing and reviewing this collection of information. Send comments regarding this burden estimate or any other aspect of this collection of information, including suggestions for reducing this burden to Department of Defense, Washington Headquarters Services, Directorate for Information Operations and Reports (0704-0188), 1215 Jefferson Davis Highway, Suite 1204, Arlington, VA 22202-4302. Respondents should be aware that notwithstanding any other provision of law, no person shall be subject to any penalty for failing to comply with a collection of information if it does not display a currently valid OMB control number. **PLEASE DO NOT RETURN YOUR FORM TO THE ABOVE ADDRESS.**

1. REPORT DATE *(DD-MM-YYYY)* 26-02-2007	2. REPORT TYPE TECHNICAL PAPER	3. DATES COVERED *(From - To)* 20 Sep 2005 - 22 Sep 2006
4. TITLE AND SUBTITLE The Multi-Lens Array Architecture		5a. CONTRACT NUMBER IN-HOUSE
		5b. GRANT NUMBER
		5c. PROGRAM ELEMENT NUMBER 62204F
6. AUTHOR(S) Danh Luu		5d. PROJECT NUMBER 4916
		5e. TASK NUMBER HA
		5f. WORK UNIT NUMBER 01
7. PERFORMING ORGANIZATION NAME(S) AND ADDRESS(ES) AFRL/SNHA Air Force Research Laboratory 80 Scott Drive Hanscom AFB MA		8. PERFORMING ORGANIZATION REPORT
9. SPONSORING / MONITORING AGENCY NAME(S) AND ADDRESS(ES) Electromagnetics Technology Division SOURCE CODE: 437890 Sensors Directorate Air Force Research Laboratory 80 Scott Drive Hanscom AFB MA 01731-2909		10. SPONSOR/MONITOR'S ACRONYM(S) AFRL-SN-HS
		11. SPONSOR/MONITOR'S REPORT NUMBER(S) AFRL-SN-HS-TP-2006-1036

12. DISTRIBUTION / AVAILABILITY STATEMENT
APPROVED FOR PUBLIC RELEASE; DISTRIBUTION UNLIMITED; ESC 06-1036, DATE 11 Sep. 06

13. SUPPLEMENTARY NOTES
Published in Proceedings of the 2006 Antenna Applications Symposium, Monticello, Illinois, 20 September 2006, p 429-454

14. ABSTRACT
As communication and radar systems migrate toward wider bandwidths, the quantization lobes inherent in conventional phased array systems manifest as one of the foremost challenges for array designers who must consider not only the need for a large and inexpensive array with wideband requirements but also practical issues, such as the ease of transporting and realizing such an array. Large phased arrays based on conventional subarray architecture, with time delays at the subarray level, exhibit very high quantization lobes when scanned over a wide bandwidth. This paper describes a multi-lens (ML) array architecture that is suitable for very large arrays with wideband (bandwidth to center frequency ratio greater than 0.2) scanning requirements. In addition to having low quantization lobes, the ML array architecture is modular, scalable, and compact in volume. The proposed architecture approximates the ideal gradient time delay network with a combination of time delays at the subarray level, time delays of Rotman lenses, and small phase shifts. The basic idea behind the ML architecture is to concatenate multiple modified Rotman lenses together to form a large array with non-periodic phase settings across the large array to lessen the accumulation of quantization lobes at any specific angle.

15. SUBJECT TERMS
Antennas, phased arrays, digital beamforming, millimeter waves, antenna measurements

16. SECURITY CLASSIFICATION OF:			17.LIMITATION OF ABSTRACT	18.NUMBER OF PAGES	19a. NAME OF RESPONSIBLE PERSON Danh Luu
a. REPORT Unclassified	b. ABSTRACT Unclassified	c. THIS PAGE Unclassified	UU	26	19b. TELEPHONE NUMBER *(include area code)* N/A

Standard Form 298 (Rev. 8-98)
Prescribed by ANSI Std. Z39.18

i

The Multi-Lens Array Architecture.

Danh Luu
AFRL/SNHA

Abstract: As communication and radar systems migrate toward wider bandwidths, the quantization lobes inherent in conventional phased array systems manifest as one of the foremost challenges for array designers who must consider not only the need for a large and inexpensive array with wideband requirements but also practical issues, such as the ease of transporting and realizing such an array. Large phased arrays based on conventional subarray architecture, with time delays at the subarray level, exhibit very high quantization lobes when scanned over a wide bandwidth. This paper describes a multi-lens (ML) array architecture that is suitable for very large arrays with wideband (bandwidth to center frequency ratio greater than 0.2) scanning requirements. In addition to having low quantization lobes, the ML array architecture is modular, scalable, and compact in volume. The proposed architecture approximates the ideal gradient time delay network with a combination of time delays at the subarray level, time delays of Rotman lenses, and small phase shifts. The basic idea behind the ML architecture is to concatenate multiple modified Rotman lenses together to form a large array with non-periodic phase settings across the large array to lessen the accumulation of quantization lobes at any specific angle.

1. INTRODUCTION

A. Quantization Lobes of Phased Array Systems.

Although wide-angle, high bandwidth, electronic scanning arrays are highly desirable, the present cost to build large arrays with such capabilities is prohibitive, since a time delay unit is required behind each element of an *ideal* wideband array. Subarraying to reduce the number of time delay units (and receivers) is a conventional approach to cut cost in a narrowband system. However, as we increase the bandwidth, the performance of the conventional subarray architecture degrades catastrophically due to the rising quantization (grating) lobes that have buried themselves beneath the sidelobes in the narrowband system but rise rapidly with increasing bandwidth. While we cannot live with these undesirable quantization lobes, we cannot live without them since they are natural companions of the various periodic aspects of the array, which enable us not only to reduce the fabrication cost and complexity of the array but also to simplify the array's analysis and controls.

B. Motivation behind the Multi-Lens (ML) architecture.

Under ideal assumptions (isotropic radiators, $\lambda/2$ spacing, uniform illumination, etc.), the far field antenna pattern is the Fourier transform of the aperture distribution across the surface of the array. The applied phase settings of the conventional subarray can be decomposed into two terms: the ideal phase term and the phase error term,

$$AF(\theta) = \sum_{n=0}^{N-1} e^{jn\pi \sin(\theta)} e^{-j\alpha_n} = \sum_{n=0}^{N-1} e^{jn\pi \sin(\theta)} e^{-j\beta_n} e^{-jE_n}, \tag{1}$$

where

$$\alpha_n = \beta_n + E_n,$$
$$\beta_n = n\pi \sin(\theta_0).$$

E_n is the phase errors at the nth elements, β_n is the ideal phase settings for scanning to θ_0, and α_n is the applied phase.

From the modulation property of the Fourier transform and with $\exp(-j\beta_n)$ playing the role of the modulator, another way to compute the array pattern would be to take the error pattern, computed from the phase errors $\exp(-jE_n)$, and shift it to θ_0.

When using conventional subarrays with narrowband systems (small array size and small bandwidth), the phase errors E_n are zero or nearly zero, and so the array pattern is simply a broadside beam shifted to θ_0. However, when using a conventional subarray in a system with considerable bandwidth, the phase errors are not all zero and in general produce a plot similar to the phase errors plot shown in Figure 1.
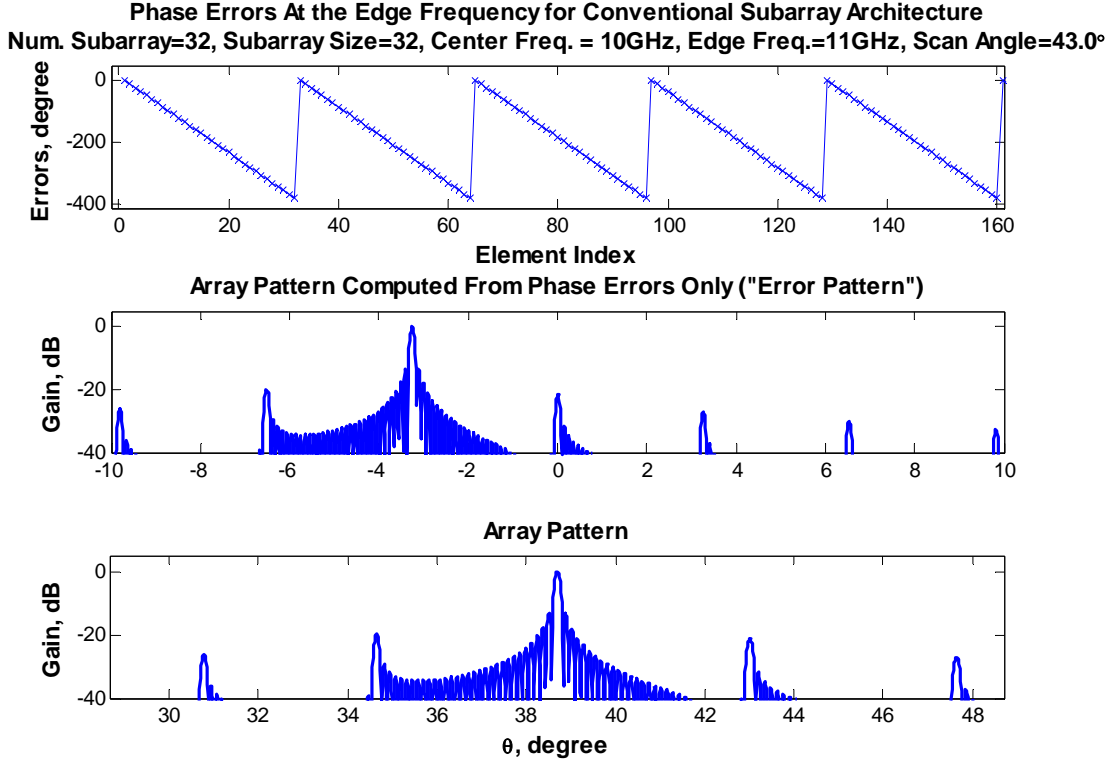

Figure 1. Phase errors and the array patterns corresponding to the applied phase. The phase errors and the array patterns were computed at the edge frequency for an array based on the conventional subarray architecture. The phase errors are shown for the first 160 elements of the array.

Unlike the zero bandwidth case, the error pattern of the edge frequency in the wideband case also has, in addition to the main beam at broadside, quantization lobes due to the periodic phase errors, E_n. The heights of these quantization lobes are generally related to the heights (maximum value) of the phase errors and the period of these quantization lobes is related inversely to the period of the phase errors. Since the phase error is a linear function of $\sin(\theta_0)$, at broadside scan ($\theta_0 = 0$) the phase errors are zero and as θ_0 increases the phase error also increases.

The ML array architecture to be discussed reduces the quantization lobes by reducing the phase scan angle, θ_0. To smear out the grating lobe, the phase scan angle is set to different values from subarray to subarray so that looking across the array, the phase errors are non-periodic. Although there are many sources of phase and amplitude errors in the array that cause sidelobes to rise, only errors from phase shifters and array tapering are considered in this paper.
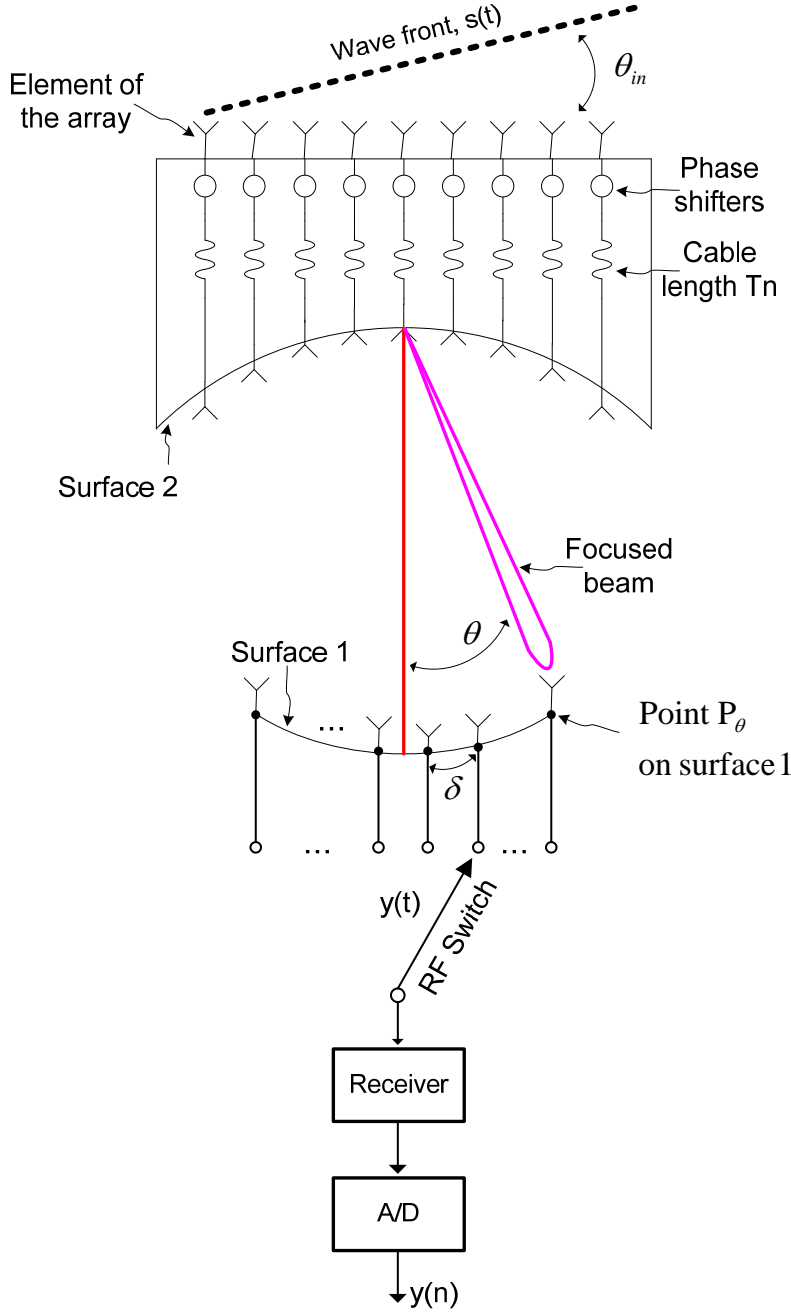
2. A SINGLE LENS.

Figure 2. An illustration of a subarray of the Multi-Lens architecture.

A. Details of a Subarray.

The ML array architecture consists of M modified Rotman lenses with the detail of each lens, or "subarray", shown in Figure 2 (the array is assumed to be used for receiving). Connecting elements of the array to the ports on surface 2 are cables of variable lengths. The element spacing on surface 2 as well as the nth cable length, T_n, are determined by three design equations derived in [4]. The constraints that lead to these design equations were written in terms of the three independent parameters in the lens: x_n, y_n (the coordinates of the nth element on surface 2) , and T_n (the time delay of the nth cable that connects from the probe at $(x_n,\ y_n)$ to the

corresponding element in the linear array aperture). Details of the three constraints were discussed in [4] and can be summarized as follows: a) path lengths of the rays tracing from the incoming planar wave-front arriving at some angle θ_{in} to the focal point P_α on surface 1 are equal, i.e., a requirement of having a perfect focus at point P_α; b) perfect focus at P_0; and c) perfect focus at point $P_{-\alpha}$. Although feed points along surface 1 between $P_{-\alpha}$ and P_α are imperfect foci, path length errors associated with these foci are small and insignificant compared to other sources of error in the array. Path length error is the difference between the maximum and the minimum lengths of the rays tracing from the incoming planar wavefront to a point on surface 1.
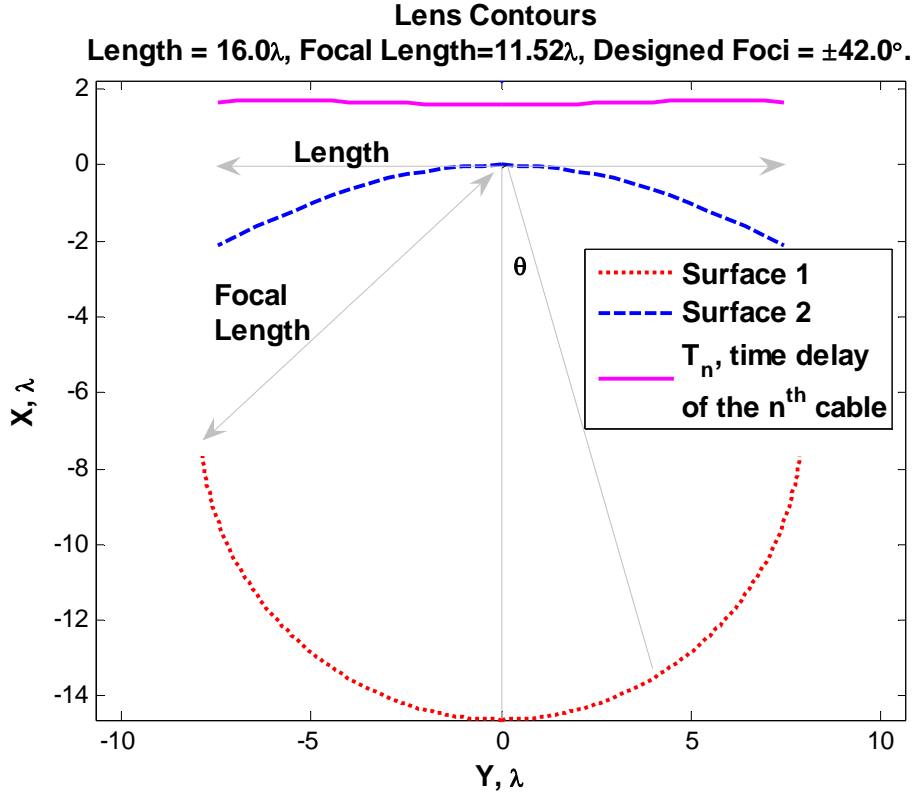
Lens Contours
Length = 16.0λ, Focal Length=11.52λ, Designed Foci = ±42.0°.

Figure 3. An illustration of the surfaces of a Rotman lens with length 16λ and foci at α = 0° and α = ±42°.
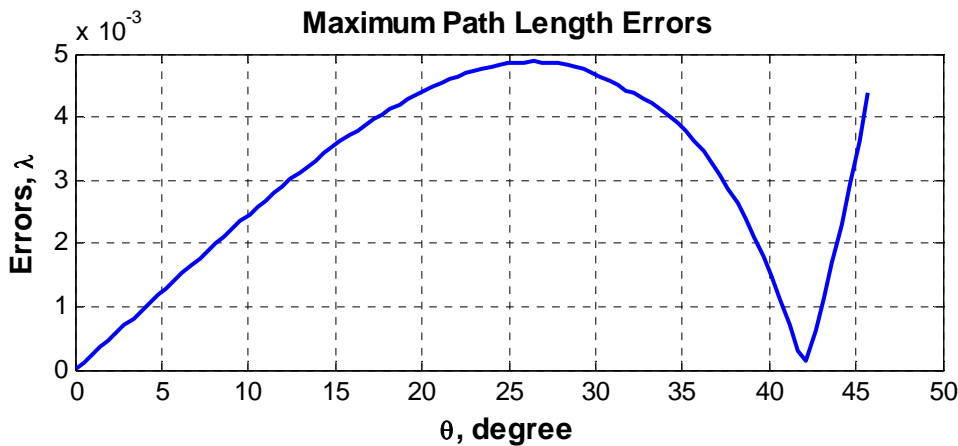
Maximum Path Length Errors

5

Figure 4. Path length errors for the foci on surface 1 of the lens in Figure 3.

For example, the two surfaces of a Rotman lens, designed with length 16λ and foci at 0 and $\alpha = \pm 42°$ are shown in Figure 3. The path length errors, shown in Figure 4, at the designed foci are zero as expected whereas the path length errors at other points on surface 1 are small and can be considered as zero.

In the ML architecture to reduce the cost and complexity of the subarray, elements on surface 1 can be spaced sparsely at δ degree intervals. Hence the phase shifters are used to focus any incoming beam between $\pm \alpha$ to the center of an element on surface 1 as illustrated in Figure 5. Although one will attempt to set δ to be as large as possible to reduce the number of elements on surface 1, if δ is set too large, phase shifters will be required to scan to wide angles, which will cause beam squint at the subarray level, and elevated grating lobes at the array level. The strategy used in this paper is to initially choose δ, such that the beam squint at the edge frequency is less than half of the 3dB beamwidth of the subarray. After δ is determined, the array pattern is computed and the maximum grating lobe is compared against the desired level to determine whether δ needs to be decreased.
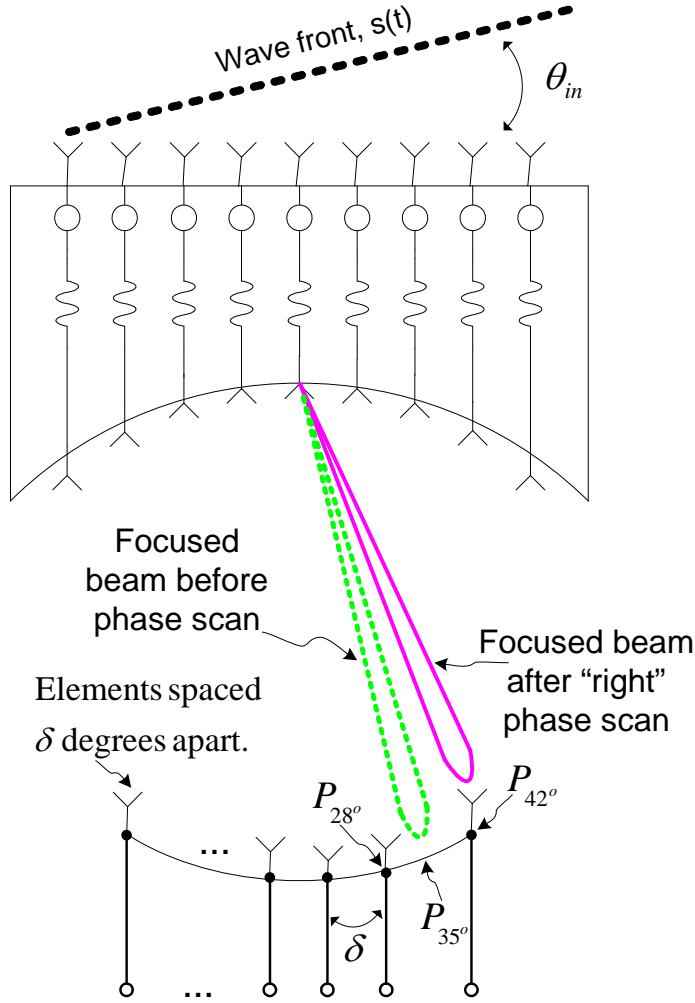
Figure 5. Phase scanning (focusing) a beam to the closest element on surface 1.

B. Computing the Far Field Subarray Pattern of a Single Lens

Suppose that the elements in the subarray lens are isotropic radiators and that a planar wavefront impinges on the array at θ_{in}. Assuming that the entire extent of surface 1 are in perfect focus, the received signal of the element located at point P_θ on surface 1 is,

$$y(t,\theta) = \sum_{n=0}^{N-1} s(t - \tau_n + w_n)e^{-j2\pi f_0 \tau_{phase}},$$

(2)

where

$$\tau_n = \frac{nd\sin(\theta_{in})}{c},$$

$$w_n = \frac{nd\sin(\theta)}{c},$$

$$\tau_{phase} = \frac{nd\sin(\theta_0)}{c},$$

$$d = \frac{\lambda_d}{2} = \frac{c}{2f_d}.$$

s(t) is the wavefront that impinges on the array, d is the distance between elements of the array, c is the speed of light, θ_0 is the phase scan angle, τ_{phase} is the phase scan, and f_0 is the center frequency.

Taking the Fourier transform of y(t, θ) with respect to time, t, yields

$$Y(f,\theta) = \sum_{n=0}^{N-1} S(f) e^{j2\pi f(-\tau_n + w_n)} e^{-j2\pi f_0 \tau_{phase}} = S(f)H(f), \tag{3}$$

where

$$H(f,\theta) = \frac{\sin(N\varphi/2)}{\sin(\varphi/2)} e^{j\frac{N-1}{2}\varphi},$$

$$\text{and } \varphi = \frac{\pi}{f_d}(f\sin\theta - f\sin\theta_{in} - f_0\sin\theta_0).$$

S(f) is the Fourier transform of s(t) and has spectral content from f_{low} to f_{high}, N is the number of elements on surface 2, and f is frequency.

The received power at point P_θ can be computed using Eq. 3,

$$\text{SAF}(\theta) = \int_{f_{low}}^{f_{high}} |Y(f,\theta)|^2 \, df \tag{4}$$

If s(t) is an ideal wideband signal, such that

$$S(f) = 1, \; f_{low} \le f \le f_{high}$$
$$S(f) = 0, \text{ otherwise}$$

Eq. 4 simplifies to,

$$\text{SAF}(\theta) = \int_{f_{low}}^{f_{high}} |H(f,\theta)|^2 \, df = \int_{f_{low}}^{f_{high}} \left| \frac{\sin(N\varphi/2)}{\sin(\varphi/2)} \right|^2 df, \tag{5}$$

which is the *subarray power pattern* that has a peak when $\varphi = 0$ and $f = f_0$. For an incoming wavefront incident at θ_{in}, with phase shifters set to scan to θ_0, the peak of the subarray pattern occurs whenever,

$$f(\sin\theta - \sin\theta_{in}) - f_0 \sin\theta_0 = 0 \qquad (6)$$

or

$$\theta_{peak} = \arcsin(\sin\theta_0 + \sin\theta_{in})$$

For a wavefront arriving at θ_{in} and subarray phase setting set to scan to θ_0, the peak of the focused beam on surface 1 is at $P_{\theta peak}$. Eq. 6 computes the required phase setting to focus an incoming beam to a specified location, $P_{\theta peak}$, on surface 1.
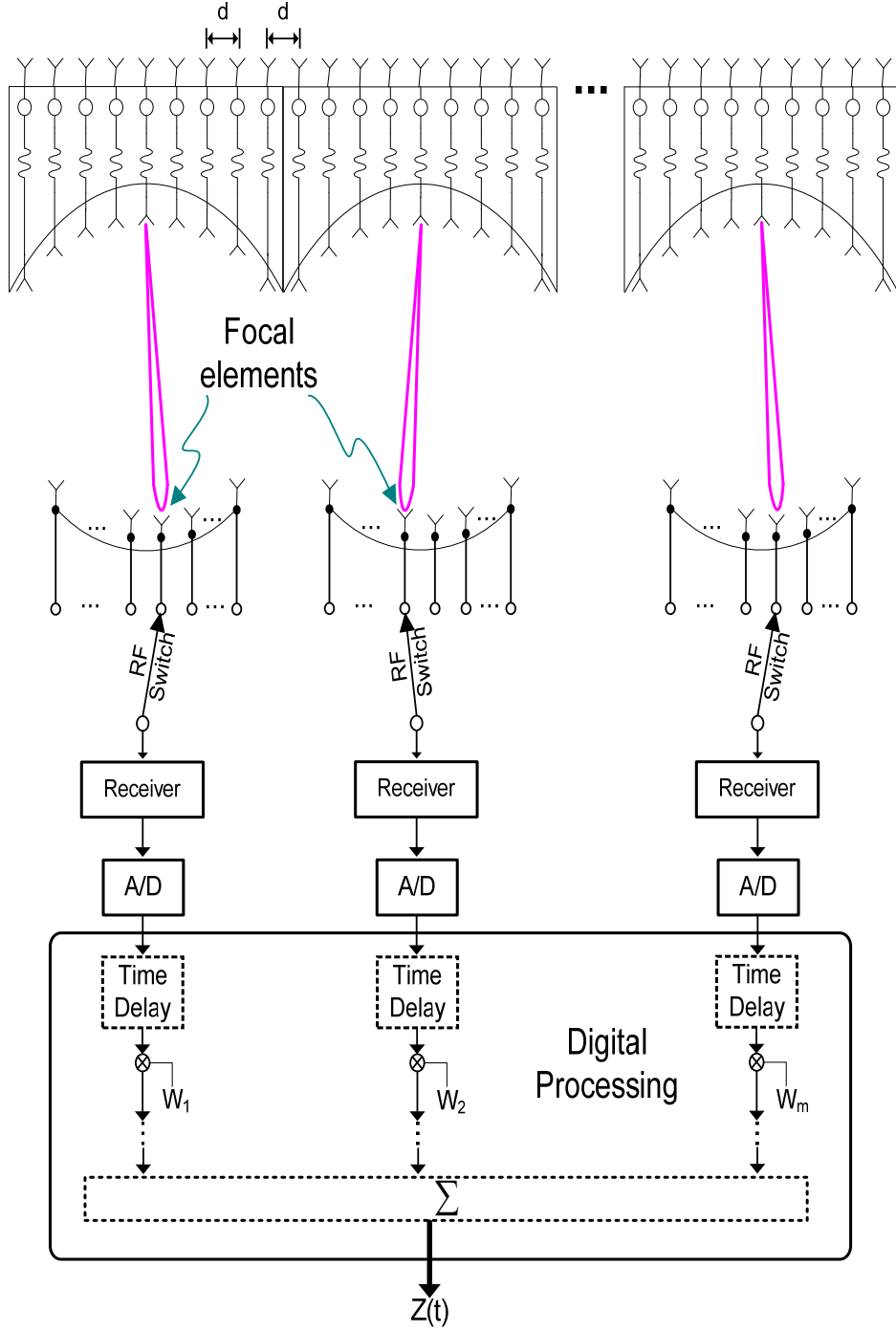
3. MULTIPLE LENSES.

Figure 6. Block diagram of the Multi-Lens architecture.

The multi-lens (ML) array proposed in this paper consists of M subarray lenses placed adjacent to each other as shown in Figure 6. In the receive case, an incoming planar wavefront impinging on the array will be focused to an element on surface 1. RF switch is used to connect the output of the element at the focal point to the input of the receiver.   After the analog to digital

conversion stage, the digital signal is weighed and time delayed using any of the techniques discussed in references [6] and [7].

A. Scattering Between Adjacent Lenses.

It is assumed that scattering between adjacent lenses is negligible in the receive case. To see why this assumption is valid, consider the lens in Figure 3 and suppose that there is a wavefront arriving at broadside. As seen in Figure 7, the separation angle, γ, between the two broadside focal points of two adjacent lenses is 48.1°. The energy that radiates from subarray 1 to subarray 2 is the sidelobe at $\gamma = 48.1°$. It will be assumed that this energy is negligible as compared to the energy of the mainlobe. Although only a broadside case is considered here, the separation angles for other scan values are as wide as in the broadside case.
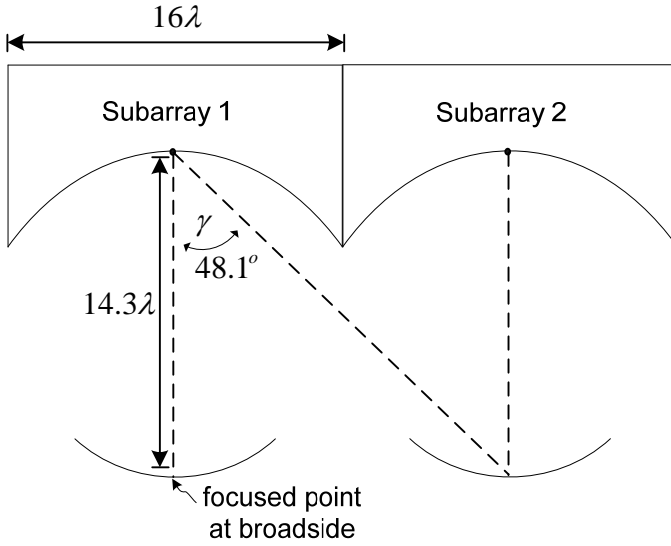

Figure 7. The separation angle γ between two focal points of two adjacent lenses.

B. Computing the Array Pattern of the Multi-Lens Architecture.

The ML array is steered using a combination of phase shifters and time delays. At the subarray level phase shifters are located between the lenses and the subarray apertures. Time delay units at the array level are located at the focal contour of each lens. As shown in Figure 6, the outputs of the M subarrays are summed, and the individual subarray's outputs $y_m(t)$ are time delayed by τ_m, then weighed with w_m. The time delay τ_m steers the subarray pattern to direction θ_{in}, while the weights w_m are used to lower the array's sidelobes to a desired level. The quantization lobe is not affected by w_m. The output signal after summing the M subarrays is,

$$z(t,\theta_{in}) = \sum_{m=0}^{M-1} w_m y_m(t + \tau_m - L_m), \tag{7}$$

where

$$D = Nd,$$

11

$$L_m = \frac{mD\sin(\theta_{in})}{C},$$

$$\tau_m = \frac{mD\sin(\theta_{in})}{C}.$$

L_m is the difference in time delay between phase centers of subarray, τ_m is the digital time delay, and D is the distance between subarray.

Unless indicated otherwise, the set of digital weights, w_m, have been selected to produce a -32 dB Chebyshev window.

Taking the Fourier transform of $z(t,\theta_{in})$ with respect to *t* we have,

$$Z(f,\theta_{in}) = \sum_{m=0}^{M-1} w_m Y_m(f)e^{j2\pi f(\tau_m - L_m)}. \tag{8}$$

Eq. 3, expressed in terms of the scan angle of the mth subarray, is given as

$$H(f,\theta_m) = \frac{\sin(N\varphi_m/2)}{\sin(\varphi_m/2)}, \tag{9}$$

where

$$\varphi_m = \frac{\pi}{f_d}(f\sin\theta^m - f\sin\theta_{in} - f_0\sin\theta_0^m).$$

θ^m is the location of the focal element on surface 1 of the mth subarray and θ_0^m is the phase scan angle at the mth subarray.

Substituting Eq. 9 into Eq. 8 we have,

$$Z(f,\theta_{in}) = S(f)\sum_{m=0}^{M-1} w_m H(f,\theta_m)e^{j2\pi f(\tau_m - L_m)} \tag{10}$$

Suppose that s(t) is an ideal wideband signal such that

$S(f) = 1, f_{low} \le f \le f_{high}$
$S(f) = 0$, otherwise

The *wideband array power pattern*, $AF(\theta_{in})$, can be computed by integrating Eq. 10 over the desired frequency range,

$$\text{AF}(\theta_{in}) = \int_{f_{low}}^{f_{high}} \left| Z(f, \theta_{in}) \right|^2$$

$$= \int_{f_{low}}^{f_{high}} \left| \sum_{m=0}^{M-1} w_m H(f, \theta_m) e^{j2\pi f(\tau_m - L_m)} \right|^2 df \tag{11}$$

$$= \int_{f_{low}}^{f_{high}} g(f, \theta_{in}) df,$$

$$\text{where } g(f, \theta_{in}) = \left| \sum_{m=0}^{M-1} w_m H(f, \theta_m) e^{j2\pi f(\tau_m - L_m)} \right|^2$$

There is no closed form solution for Eq. 11. However, since g(f) varies slowly with respect to f, numerical integration using Simpson's 1/3 Rule is a convenient method to evaluate Eq. 11. It can be shown the result can be expressed as,

$$\text{AF}(\theta_{in}) = \int_{f_{low}}^{f_{high}} g(f, \theta_{in}) df \approx \frac{h}{3} \sum_{k=0}^{2K} l_k g(f_k, \theta_{in}), \tag{12}$$

where,

$$h = f_1 - f_0,$$

$$l_k = [1, 4, 2, 4, 2, ..., 4, 1]$$

and the f_k are 2K+1 equally spaced frequency points between f_{low} and f_{high}.

The wideband array patterns in Section 4 were computed using Eq. 12 with 33 frequency points. In narrowband system, Eq. 12 will produce the same array pattern as the classical phased array pattern. However, unlike the classical array pattern, which computes the power for a single frequency, Eq. 12 computes the power of the signal s(t) at a given angle θ_{in}. So all frequencies in s(t) contribute to the quantization lobe of the wideband power pattern.

4. EXAMPLES

The examples below demonstrate the wideband scanning feature of the ML array architecture. Although one would not normally use a conventional subarray for wideband scanning, the examples shown in Section 4A illustrate the severity of the quantization lobes associated with phase scanning in a large wideband conventional subarray.

A. Conventional Subarray

The array pattern for an array of 1024-elements based on the conventional subarray architecture is shown in Figure 8 at 43° scan. In this case, phase shifters are located behind each element, time delay units are located behind each of the 32 subarrays. The array in section 4A, 4B and 4C have an operating bandwidth of 2 GHz centered at 10 GHz and are assumed to have uniform tapering and ideal phase shifters with infinite accuracy. As expected, the peak quantization lobe is approximately 5 dB down from the main beam. The power pattern of the conventional subarray was computed using Eq. 11 with $\theta_0^m = 43^o$ for all subarrays.

**Power Pattern for a Conventional Subarray With 32 Subarrays Each With 32 Elements
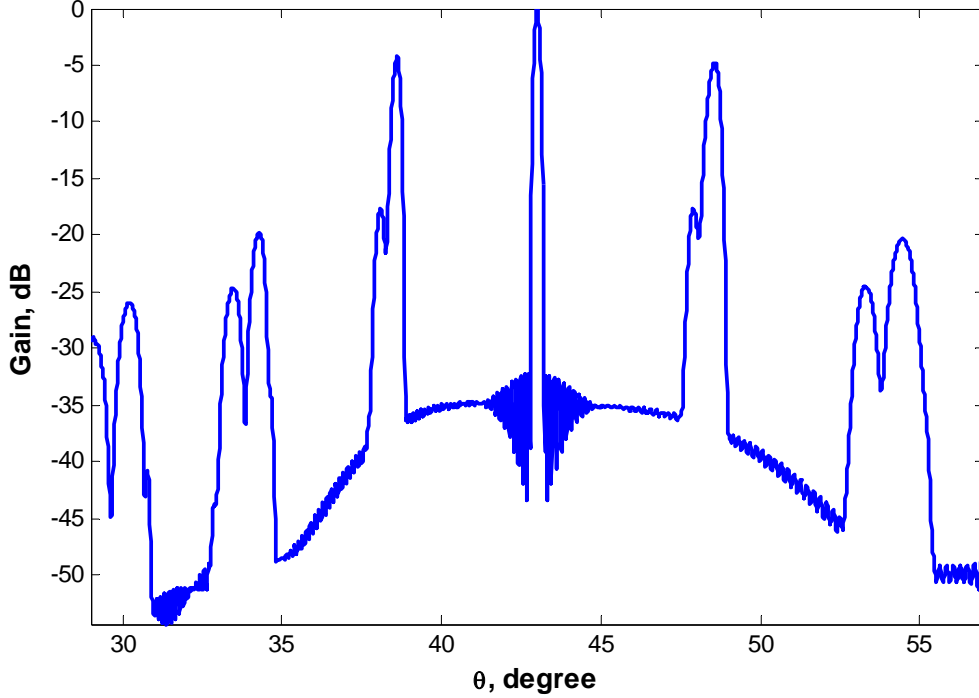ScanAngle = 43°, Operating Freq. = 9 to 11 GHz**

Figure 8. Wideband array pattern for an array of 32 subarrays, each with 32 elements, using a contiguous subarray architecture. The scan angle is 43° over a 2 GHz bandwidth, at a center frequency of 10 GHz.

B. An Array Based on Multi-Lens Array Architecture

The ML array architecture lowers quantization lobes by reducing and randomizing phase errors across the array. In addition to exhibiting low grating lobes, the ML architecture consists of M distinct and detachable subarray sections, which are modular and fairly compact in depth. For example, a 1024-element ML array with 32 subarrays has a focal length of $32*(\lambda/2)*0.72 = 11.52\lambda$, whereas an equivalent Rotman lens, would have a focal length of $1024*(\lambda/2)*0.72 = 368.64\lambda$, which is physically impractical.

In the cases shown in Figure 9, the ML array has 32 subarray lenses, each with 32 elements equally spaced ($d = \lambda/2$). The operating parameters are the same as in Section 4A. The desired sidelobe level is -29 dB for all scan angles between ±45°. To achieve this low sidelobe level, elements on surface 1 of each subarray are placed at ±42, ±28, ±14 and 0 degrees so that phase shifters scan the beam to a maximum value of $\delta = 14°$. In most cases, the phase scan angle will be less than $\delta/2 = 7°$. The grating lobe level in the ML array increases or decreases with increases or decreases in the distance δ between adjacent elements on surface 1.

Unlike the conventional subarray architecture, where the maximum grating lobe occurs at the highest scan angle, the peak grating lobes in the ML architecture generally occur when the incoming planar wavefront is focused to a point P_θ that is in between any two elements on

surface 1. For the current example, these points are ±7, ±21, and ±35 degrees. Suppose that the incoming wavefront is focused by the subarray lens to point $P_{35°}$ as shown in Figure 5. Using phase shifters, we have the option to scan the beam either to the element located at $P_{42°}$ (right scan) or to the element located at $P_{28°}$ (left scan). To make the phase errors non-periodic across the array which smears out the grating lobes, the decision to scan to the left or to scan to the right at each subarary is based on a randomly chosen binary string of length M. Details of a simple scheme that chooses the "random sequence" shown in Figure 9a are discussed in Appendix A. In this scheme, a '0' in the mth position represents a left scan at subarray m and a '1' represents a right scan. With random scanning, the peak grating lobe at $35°$ scan is about -30.2dB, which is significantly lower than the -24.6 dB peak grating lobe that occurs in the non-random scanning case (not shown) with random sequence = "00...0".

Figure 9c shows the case where random scanning cannot be used. When the incoming beam is focused to point $P_{45°}$, there is only one element next to the focal point and the only possible scan angle is the left scan to the element at $42°$. Although the peak quantization lobe at -32.7 dB is not smeared out in this case, it is still very low since the phase scan angle is only $3°$.

Array pattern of 1024-elements array (32 lenses) based on the ML architecture. ScanAngle=35°, RandomSequence=00111000110011101101111100000101.
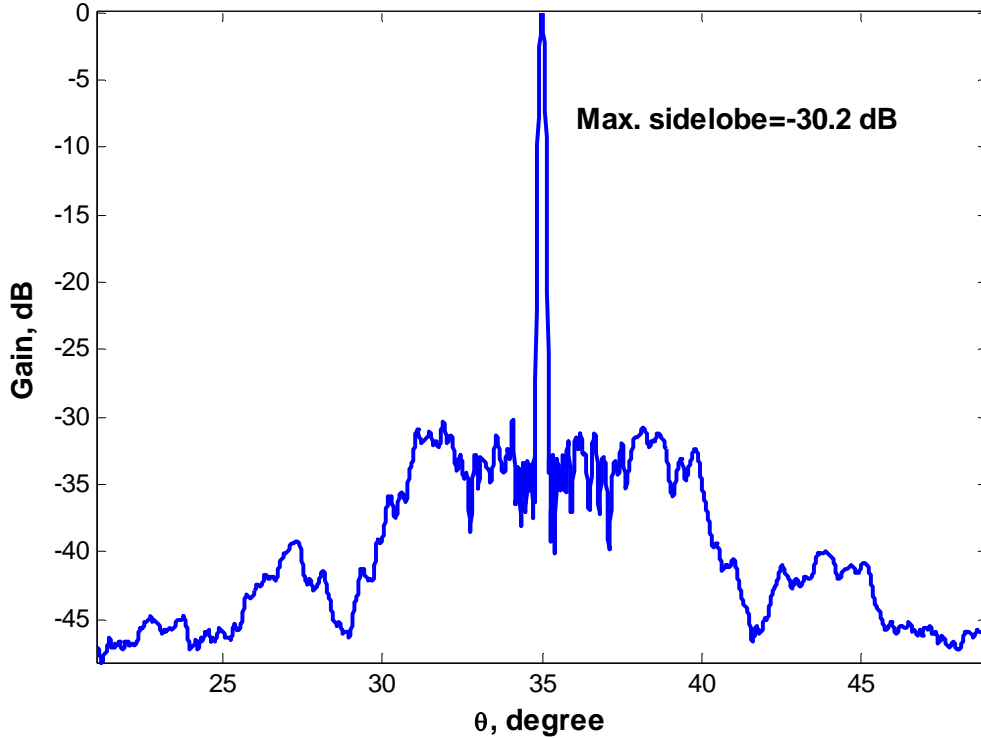

Figure 9a. Wideband array pattern of a 1024-element array based on the Multi-Lens architecture. The ML array consists of 32 subarray lenses which are scanned to different angles over a 2 GHz bandwidth centered at 10 GHz. The scan angles ($\theta = 35°$, $7°$, and $45°$) were chosen to illustrate the worst cases quantization lobe level.
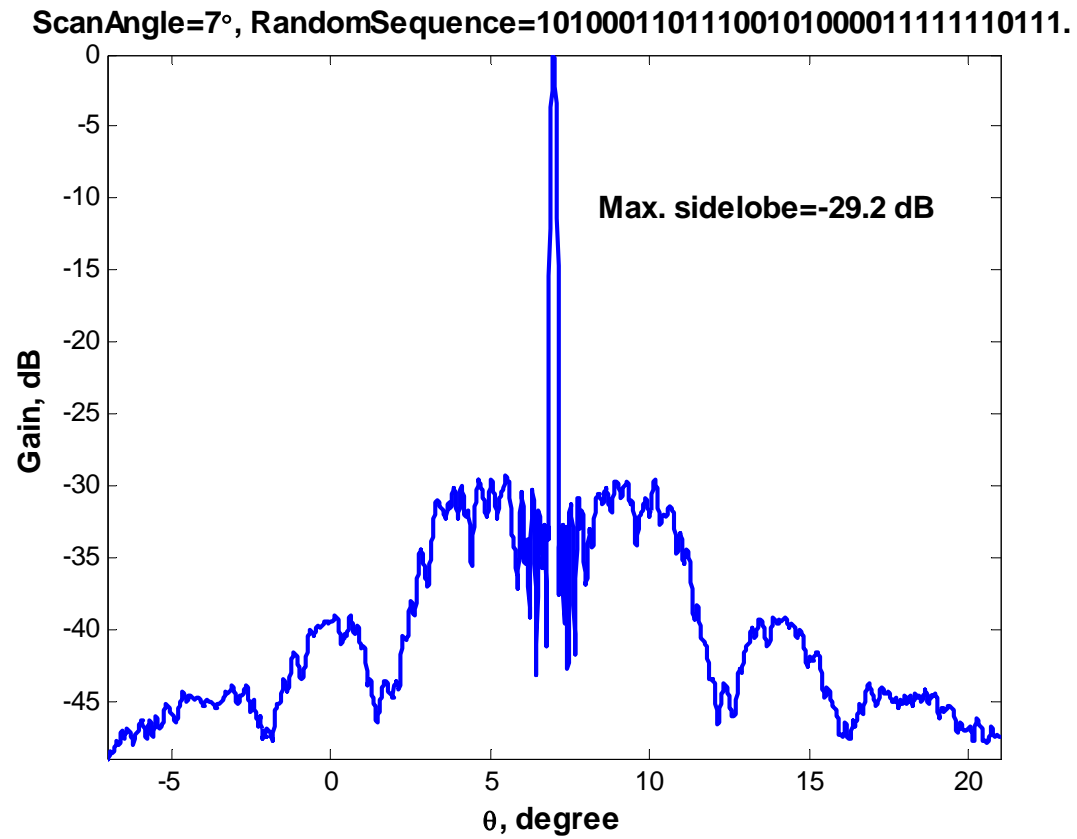
Figure 9b. Wideband array pattern for 7° degree scan.

ScanAngle=45°, RandomSequence=0000000000000000000000000000000.
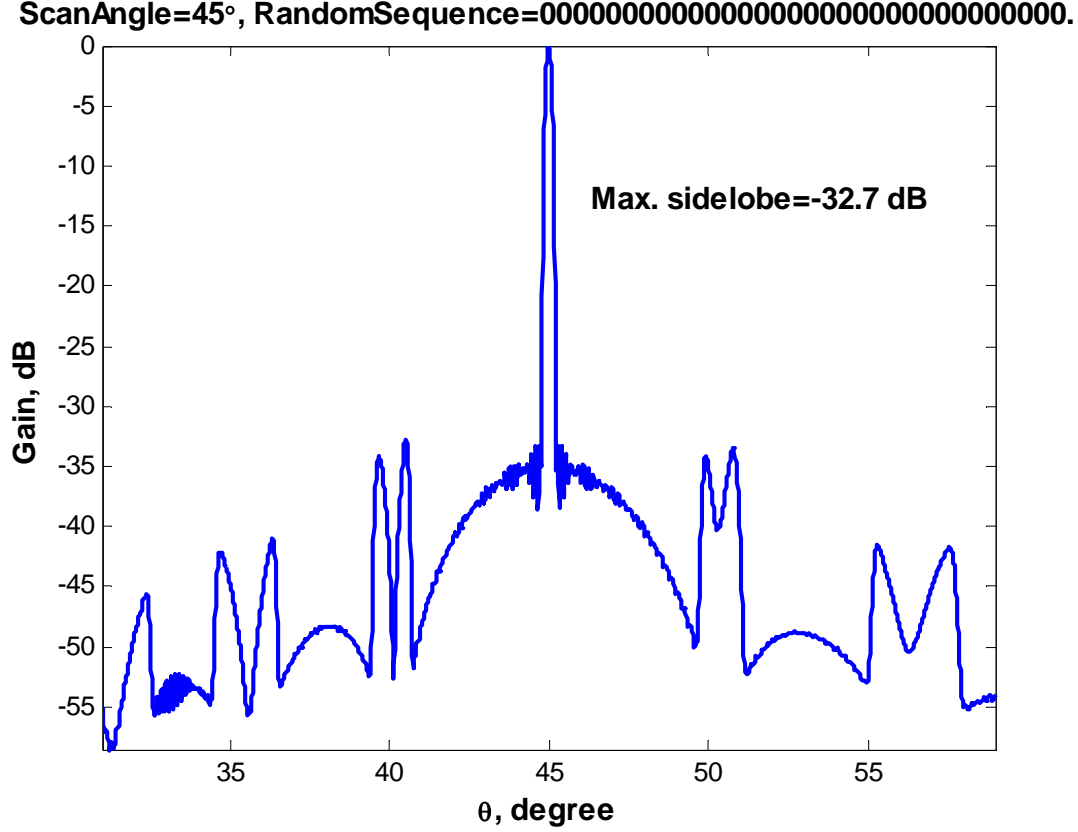

Figure 9c. Wideband array pattern for 45° degree scan. Random sequence equal to "00…0" means *left scan* at all subarrays.

C. Increasing the Size of an ML Array

Because the ML array architecture is scalable, an existing array can be enlarged by adding more lenses to the array, which suggests that the ML array architecture may be practical for large space-borne array systems. In addition to increasing the array's size, adding more subarray lenses will also lower the peak grating lobes due to the reduction in width of grating lobes and the random phase scanning scheme, which smears out the grating lobes more evenly. To demonstrate this aspect of the ML architecture, the number of subarrays in Section 4B is doubled from 32 to 64. Even though the size of the array is increased from 512λ to 1024λ, the depth of the array remains unchanged at $11.5\,\lambda$. As with convention subarray architecture, the reduction in height of the peak grating lobe occurs with increasing numbers of subarrays. However, in the ML architecture, the combination of smeared grating lobes that result from random phase scanning, and narrowed grating lobe widths, yield significantly better array patterns as shown in Figure 10.

17

Array pattern of 2048-elements array (64 lenses) based on the ML architecture.
RandomSequence=11110000111010100111111110000000001101000010011000111101010101010100.
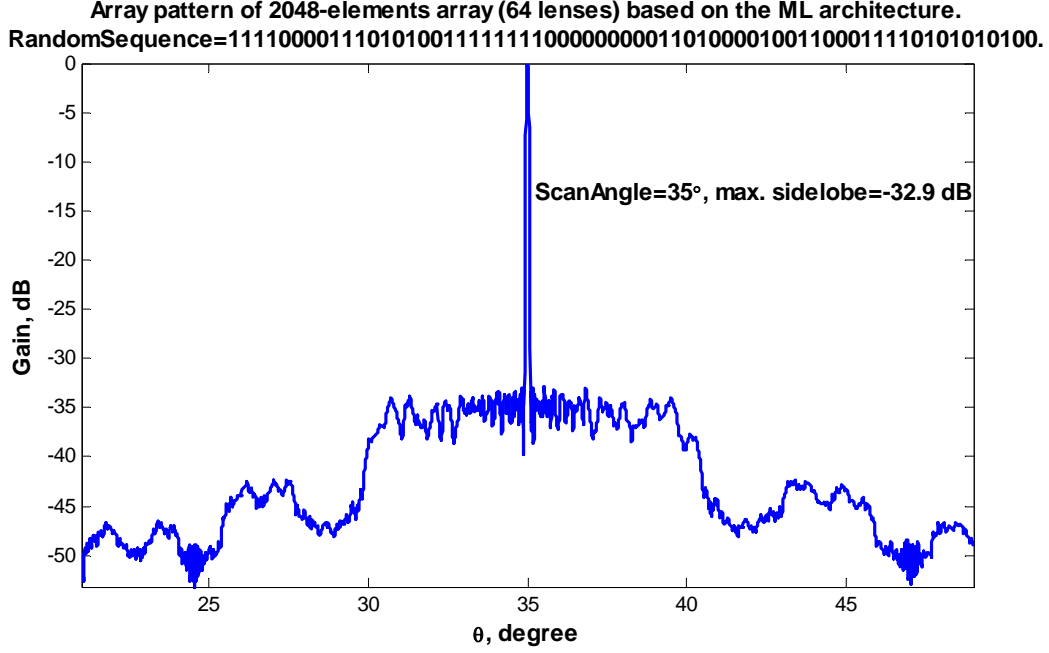

Figure 10a. Wideband array pattern of a 2048-element array based on the Multi-Lens architecture. The ML array consists of 64 subarray lenses which are scanned to different angles over a 2 GHz bandwidth centered at 10 GHz.
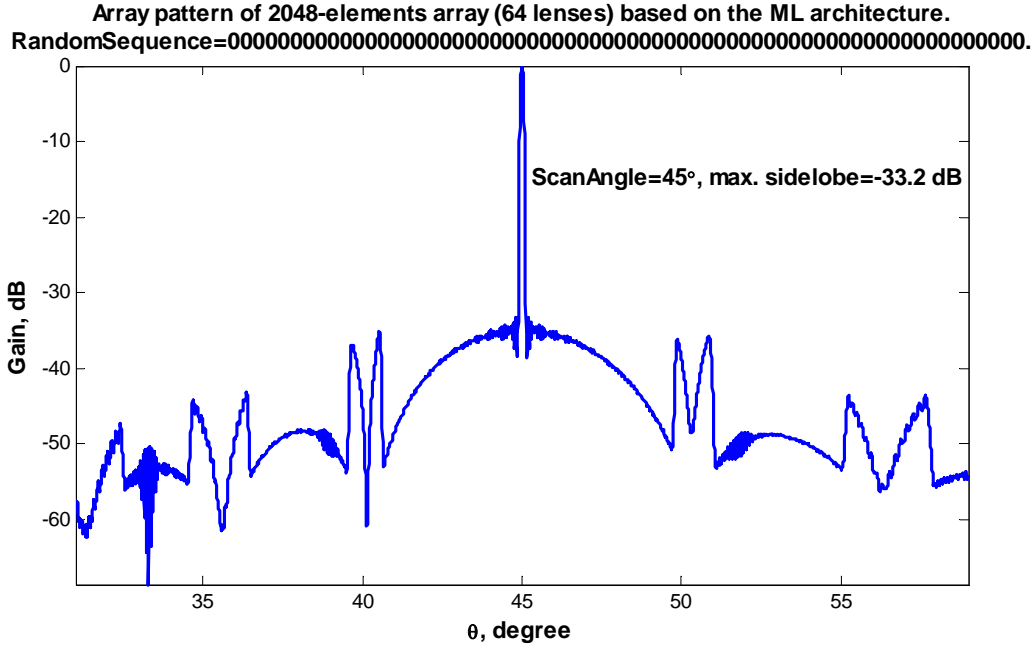
Array pattern of 2048-elements array (64 lenses) based on the ML architecture.
RandomSequence=000000000000000000000000000000000000000000000000000000000000000000.

Figure 10b. Wideband array pattern for 45° scan.

D. Phase Quantization and Subarray Tapering.

In practice, there will be some amplitude tapering across the subarray. In addition, phase shifters generate only a finite number of discrete phase states. Using 4-bits phase shifters instead of ideal

phase shifters in the ML array of Section 4B, causes the maximum grating lobe to rise by only a fraction of a dB. Although phase quantization does not have a significant effect on the maximum grating lobe level, subarray tapering will cause grating lobes to rise modestly with respect to the phase quantization case, especially in situations where random scanning cannot be used.

It is widely known that the significant effect of adding cosine tapering to a subarray is a widening of the subarray's beam width while its sidelobes are lowered. The elevated grating lobes in a tapered subarray system are caused by the shifts of the subarray pattern nulls away from the ideal locations where the grating lobes appear. Because of this misalignment, the subarray nulls are only able to partially suppress grating lobes. With greater shifting of the subarray pattern nulls, more misalignments occur and even higher grating lobe result.

At 35° scan, the peak sidelobe level of the cosine tapered array is about 2.7 dB higher than the peak sidelobe of the non-tapered array pattern, as shown in Figure 11a. The general sidelobes of the tapered array, however, are slightly lower than the sidelobes of the non-tapered array. The weights that were applied to the tapered array were computed from

$$c_n = \cos(\chi_n),$$

where

$$\chi_n = -35, -(35 + 70/31), -(35 + 140/31), \ldots, 35 \text{ degree.}$$
c_n is the weight for the nth element of the subarray.

The same random sequence, optimized for the non-tapered case, was used for both the tapered and non-tapered array. When optimized random sequences were used with both the tapered and non-tapered arrays, the peak quantization lobes in the two cases are about the same. However, without random scanning, the quantization lobes of the tapered array, shown in Figure 11b, are much higher than those of the non-tapered array. This example demonstrates another feature of the ML architecture with random scanning, which is not only able to smear out grating lobes due to periodic phase error but also due to periodic amplitude error. The amplitude error in this example is the difference between the ideal uniform taper and the cosine taper.

Array pattern of 1024-elements array (32 lenses) based on the ML architecture.
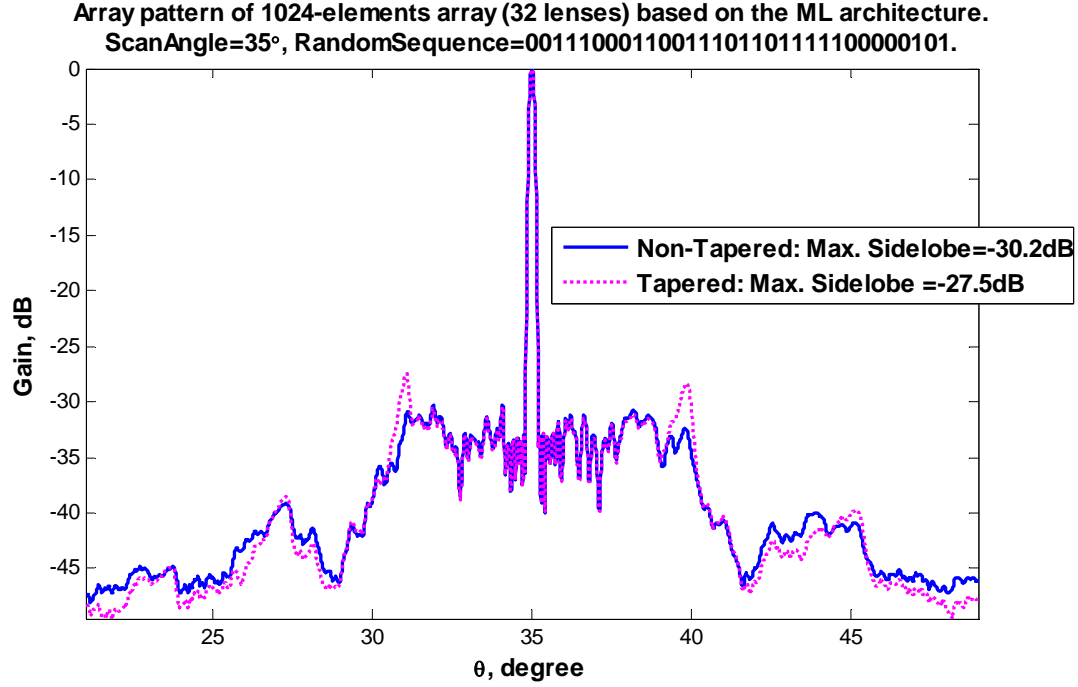**ScanAngle=35°, RandomSequence=00111000110011101101111100000101.**

Figure 11a. The wideband array patterns of an array based on the ML architecture for 35° scan. The solid line corresponds to the ML array with uniform tapering across each subarray and the dashed line corresponds to the ML array with tapered subarrays.
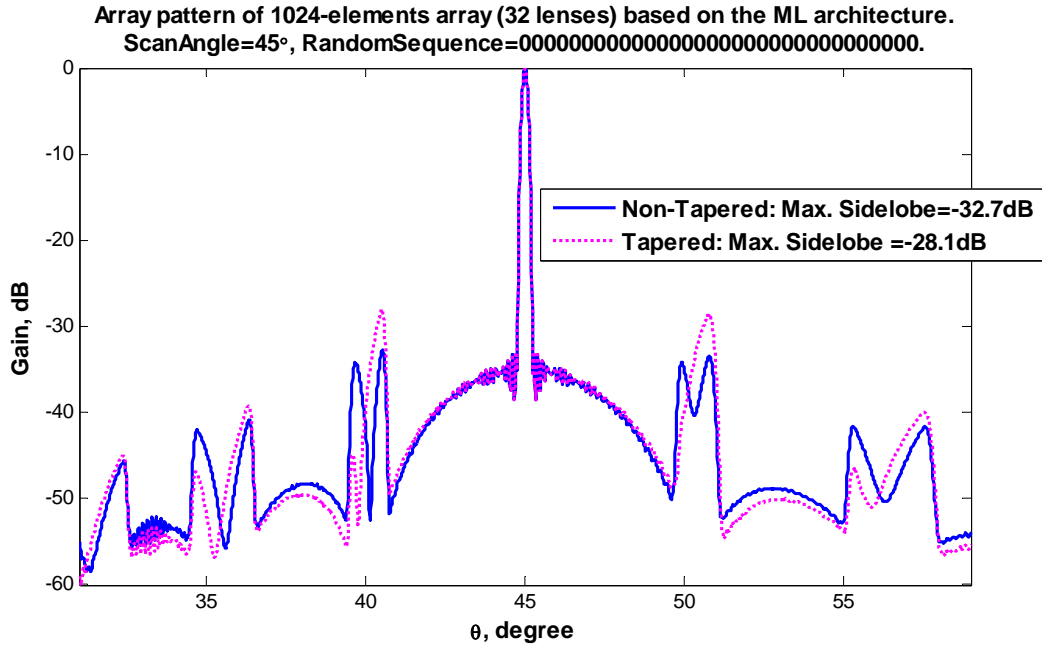
Array pattern of 1024-elements array (32 lenses) based on the ML architecture.
ScanAngle=45°, RandomSequence=00000000000000000000000000000000.

Figure 11b. Wideband array pattern for 45° scan.

5. CONCLUSION

The proposed Multi-Lens array architecture is modular, scalable and is ideally suited for very large arrays with wideband scanning requirements. Using ideal assumptions, (isotropic radiator, perfect Rotman lenses) it was shown that the quantization lobes of the ML array are much lower than the quantization lobes of a conventional subarray architecture since the ML array approximates an ideal time delay network having time delays at the subarray level, analog time delays in the Rotman lenses, and small phase approximations from phase shifters. Not only are the phase errors of the ML array much smaller than the phase errors of the conventional subarray, they are also non-periodic, which cause the grating lobes to be smeared out. To completely remove the phase errors in the ML architecture and to perhaps simplify the ML design, elements on surface 1 should be spaced closely such that phase scanning is not required. Although phase shifters can be removed from the ML architecture in this case, the complexity of the RF switching network must be increased to accommodate for the increasing number of elements on surface 1.

Examples that take into account phase quantization and amplitude tapering were considered. While phase quantization does not have a significant effect on the array pattern, the rising quantization lobe due to amplitude tapering can be smeared out using an optimized random sequence. Not all practical aspects of the multi-lens array architecture were considered. Among the important and practical details that were omitted are the locations for amplifiers (LNA) and the process for choosing the size of array and the size of the lens. Costs will dictate the locations and number of LNAs and desired gain, array's size and volume constraint will be used by array designers to choose size and the number of the lens in the array.

6. APPENDIX

A. Choosing a Random Sequence.

For the ML array in Section 4B with $N = 32$ subarrays, an exhausted search for the optimum random sequence requires the evaluation of 2^N scanning sequences. For large N, it is not practical to find the peak sidelobes for all 2^N different phase scan configurations and then select the optimum scan sequence that has the lowest sidelobe. Instead, a more tractable approach is to consider only a small subset of the 2^N scan sequences. A distribution of the peak sidelobes of the 2^N scanning sequences is first estimated to find out the size, K, of this subset and how the lowest sidelobe from the K randomly chosen sequences compared with the sidelobe of the globally optimum scan sequence. The histogram shown in Figure 12 for the array in section 4B is computed from 4200 randomly generated scanning sequences with the probability of "left" scan equal to the probability of "right" scan at each subarray.

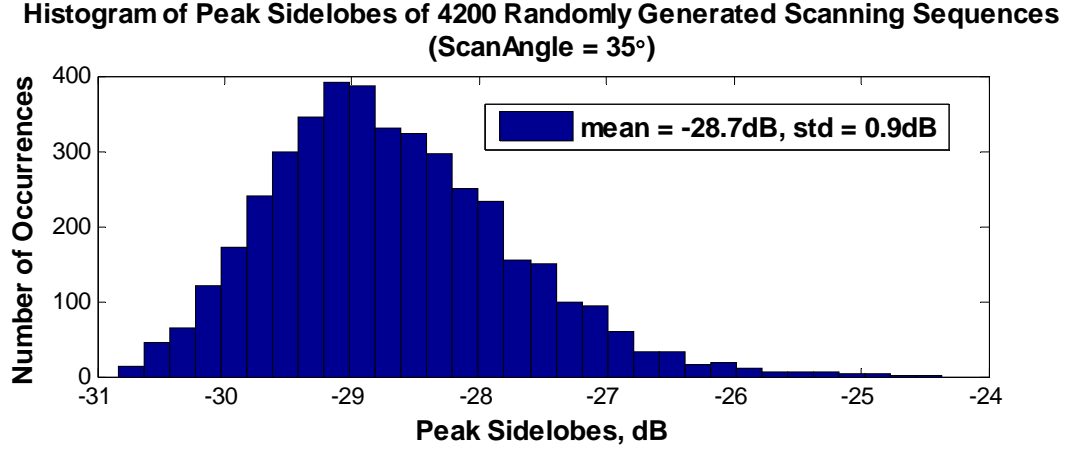**Histogram of Peak Sidelobes of 4200 Randomly Generated Scanning Sequences (ScanAngle = 35°)**

Figure 12. Histogram of the peak sidelobes of the ML array in Section 4B computed from 4200 random scanning sequences.

From the histogram, the probability of getting a random scan sequence with sidelobes level below -31 dB is very small. However, it is possible to obtain a sequence with sidelobes below -30 dB with relatively few trials. The number of trials that will be required can be determined by first estimating the probability, P_s, of a sequence with sidelobes below -30 dB. From the 4200 randomly generated sequences, a total of 264 scanning sequences exist which have sidelobes below -30 dB. The rough estimate of P_s is $264/4200 = 0.0629$ (99% margin error = ±2%) and the estimated probability of having sidelobes greater than -30 dB is,

$$P_f = 1 - P_s = 0.937.$$

Assuming that the *probability of success*, P_s, is known, the number of trials, K, required to guarantee a desired probability, P_d, of having at least one success or having at least one scanning sequence with sidelobes below -30 dB must be determined. For independent trials and $P_d = 0.99$, K can be computed from

$$0.99 = 1 - P_f^K.$$

For $P_f = 0.937$, there is a 99% chance that from the K = 71 randomly generated sequence that at least one random scanning sequence will have peak sidelobe below -30 dB.

B. Choosing Random Sequences For a Range of Scan Angles.

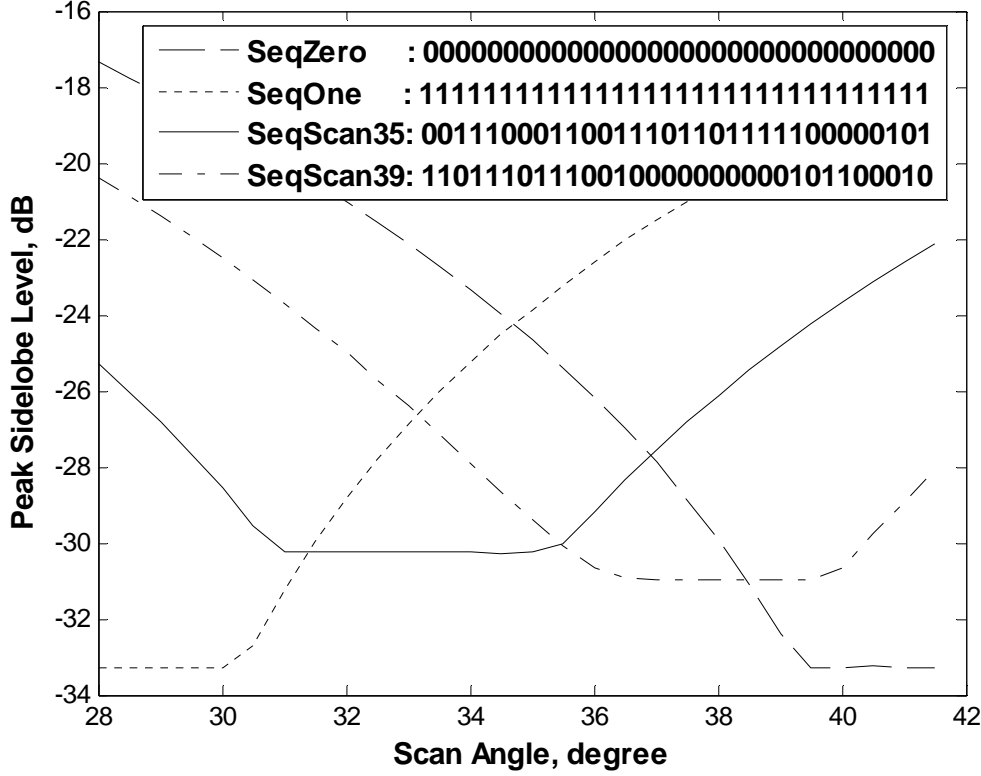**Peak Sidelobes for 4 Scanning Sequences For Use at Different Scan Angle**

Figure 13. Peak sidelobes of an ML array scanned to different angles using a random sequence that was designed for any specific angle.

Although a random scanning sequence is chosen for a specific scan angle, it can be used for scan angles that are near the optimized angle. For example, in Figure 13, the scan sequence ("SeqScan35") which was chosen for a 35° scan can be used for scan angles ranging from 31° to 35° and the resulting sidelobe level will still be below -30 dB. Two pre-computed random sequences are needed to cover 28 to 42 degrees scan for the array in Section 4B since different scan regions require different random sequences. *SeqScan35* is used for 32 to 35 degrees scanning and *SeqScan39* is used for 36 to 40 degree scanning. For scan angles ranging from 28 to 31 degrees, a left scan to the element at 28° is used at each subarray and a right scan to the element at 42° is always used for scan angle from 40 to 42 degrees.

REFERENCES

[1] W. Rotman, P. Franchi, "Cylindrical Microwave Lens Antenna for Wideband Scanning Application", Antennas and Prop. Int. Symposium, vol. 18, pp. 564-567, Jun 1980.

[2] H. L. Southhall, D. T. McGrath, "An Experimental Completely Overlapped Subarray Antenna", IEEE Trans. On Antennas and Prop. vol. AP-34, pp. 465-473, Apr 1986.

[3] R. J. Mailloux, "A Low-Sidelobe Partially Overlapped Constrained Feed Network for Time-Delayed Subarrays.", IEEE Trans. on Antennas and Prop., vol. AP-49, pp. 280-291, Feb 2001.

[4] W. Rotman, R. F. Turner, "Wide-Angle Microwave Lens for Line Source Applications", IEEE Trans. On Antennas and Prop., vol. AP-11, pp. 623-632, Nov 1963.

[5] R. J. Mailloux, "Phased Array Antenna Handbook", Artech House, 1994.

[6] T. I. Laakso, V. Valimaki, M. Karajalainen, and U. K. Laine, "Splitting the Unit Delay", IEEE Signal Processing Mag., Vol. 13, Issue 1, pp. 30-60, Jan. 1996.

[7] T. I. Laakso, T. Saramaki, and G. D. Cain. "Asymmetric Dolph-Chebyshev, Saramaki, and transitional windows for fractional delay FIR filter design", Circuits and Systems. Proceedings of the Midwest Symposium on Meeting: August 13, 1995, pp. 580-583.